Radial velocity analysis of stars with debris discs

Deepak Bisht [1,2]★ and Hugh R. A. Jones[3]★

[1]*Space Research Institute, Austrian Academy of Sciences, Schmiedlstrasse 6, A-8042 Graz, Austria*
[2]*Department of Physical Sciences, Indian Institute of Science Education and Research Berhampur, Odisha-760010, India*
[3]*Centre for Astrophysics Research, University of Hertfordshire, Hatfield, Hertfordshire, AL10 9AB, UK*

ABSTRACT

This study aims to identify potential exoplanet signals from nearby stars with resolved debris discs. However, the high activity of many stars with debris discs limits the detection of periodic signals. Our study is constrained to a sample of 29 stars that have appropriate radial velocity data and debris disc measurements sufficient to resolve their inclination. Our results confirm and update previous findings for exoplanets around HD 10647, HD 115617, HD 69830, GJ 581, HD 22049, and HD 142091, and we identify long-term activity signals around HD 207129 and HD 202628. We utilize the inclination angles of the debris discs, assuming co-planarity between debris disc and exoplanet orbit, to determine the 'disc-aligned' masses of radial velocity exoplanets in this study. The 'disc-aligned' masses of HD 69830 b, HD 69830 c, and 61 Vir b suggests that they may be classified as 'hot' or 'warm' Jupiters and so might be nearby examples of planets that have undergone recent type-II disc migration.

Key words: techniques: radial velocities – exoplanets – planet–disc interactions – circumstellar matter – planetary systems.

1 INTRODUCTION

The discovery of planets orbiting stars outside our Solar System has transformed our understanding of the cosmos. Exploring these exoplanets is vital for unraveling the diversity of planetary systems. This research is driven by the quest to identify and characterize exoplanets within resolved debris discs surrounding nearby stars. Debris discs are circumstellar structures composed of dust and debris that encircle stars. These discs consist of small particles ranging from micrometres to centimetres and are believed to originate from the collision and erosion of planetesimals, remnants of planetary building blocks, during the early stages of planetary system formation (Chambers 2004).

Debris discs are commonly observed around both young and mature stars, offering valuable insights into the evolutionary processes of planetary systems (Krivov 2010). These discs probably have two distinct phases. Initially, a protoplanetary disc consisting of gas and dust develops around a young star, followed by the gradual dissipation of the protoplanetary material after planet formation. This process results in the formation of a debris disc, which is composed of planets and residual planetesimal material (Wyatt & Jackson 2016). As a result, debris discs present an opportunity to examine mature planetary systems that could potentially harbour additional exoplanets (Milli et al. 2017; Pérez et al. 2019; Pearce et al. 2022).

The detection of debris discs and the material within them presents challenges due to the variability within the debris disc as well as that of the surrounding environment (Beichman et al. 2006). Various techniques have been developed to detect and study debris discs,

including direct imaging, particularly in the infrared and at longer wavelengths (Kilic et al. 2005). Direct high-resolution imaging of the disc structure enables detailed analysis of its properties (Schneider et al. 2014). Space-based telescopes, like the *Spitzer Space Telescope* and the *Herschel Space Observatory*, along with ground-based observatories, such as ALMA, VLT, and the Keck Observatory, have been instrumental in detecting and analysing debris discs (Nelson et al. 1985; Werner et al. 2004; Koerner et al. 2010; Pilbratt et al. 2010; Booth et al. 2016; Beuzit et al. 2019; MacGregor et al. 2022).

After Mayor & Queloz (1995) detected the first planet around a Sun-like star using the radial velocity (RV) method, over a thousand exoplanets have been confirmed using this technique (Akeson et al. 2013). Nevertheless, RV surveys encounter challenges, such as the necessity for high-precision measurements and the influence of stellar activity (Jones et al. 2006; Zechmeister et al. 2018). Additionally, accurately determining the inclination angle of a planet's orbit relative to the plane of the sky can be instrumental in RV surveys (Rivera et al. 2010; Zurlo et al. 2018). This angle can provide the true mass of a planet, yet this is not routinely available unless the planet also transits the star to provide precise knowledge of the planet's orbital parameters. In recent times, advancements in instrumentation and measuring techniques have enabled the measurement of orbital angles through astrometry. Various studies have utilized astrometric data and the RV method (Benedict et al. 2006; Xuan et al. 2020; Kiefer et al. 2021; Li et al. 2021; Llop-Sayson et al. 2021; Barbato et al. 2023; Xiao et al. 2023; Yahalomi et al. 2023) to determine the true masses of planets.

Planetary systems are recognized to form from discs surrounding young stars. Consequently, it is assumed that constituents of exoplanetary systems should exhibit a unified angular momentum direction. This implies that planets and debris discs should orbit in alignment, following the same direction, and in the same plane

★ E-mail: bishtd78@gmail.com (DB); h.r.a.jones@herts.ac.uk (HJ)

as the stellar equator (Kennedy et al. 2013). Investigations have largely indicated co-planarity or near-co-planarity between debris discs and planetary orbits. In the Solar System, for instance, the orbital planes of the planets exhibit a close alignment with each other, as well as with the Kuiper belt. This observation suggests a scenario of planet formation within a flat protoplanetary disc. There are a number of well-studied systems in the literature; for example, the orbit of β Pic b is determined to be nearly aligned with the disc mid-plane, with a tilt angle of approximately 2.4° (Matrà et al. 2019). Additionally, it closely aligns with both the stellar spin axis (Kraus et al. 2020) and the orbit of the inner planet (Nowak et al. 2020). In HR 8799 (Goździewski & Migaszewski 2018) and HD 82943 (Kennedy et al. 2013), the planets exhibit consistency in alignment with both the debris disc and the stellar spin axis. This alignment is inferred from similarities in their sky-projected inclinations. AU Mic was discovered to host a short-period transiting planet that is in alignment with its debris disc and stellar spin axis (Pallé et al. 2020; Plavchan et al. 2020). Additionally, Pearce et al. (2024) proposes that the mean motion of a planet in a coplanar disc excites debris eccentricity but does not influence the inclination angle of the debris disc. It is worth noting that existing evidence, at least for planet-hosting binaries, favours low mutual inclinations between planetary and stellar orbits (Dupuy et al. 2022) and, in contrast to determining a planet's orbital inclination, the inclination angle of a debris disc can often be deduced relatively easily from its shape and orientation relative to the star's equatorial plane (Watson et al. 2011). For our analysis, we assume a mutual inclination for the disc and planetary orbits (Kennedy et al. 2013) and calculate the disc aligned mass (M_{DA}).

It is crucial to acknowledge that there are systems where the disc and planetary orbits are misaligned (Xuan et al. 2020). Theoretical work has indicated that these misalignments could result from misaligned stellar or planetary-mass companions within the system (Nealon et al. 2019; Zhu 2019). Secular perturbations induced by companions can lead to precession in the orbits of planetesimals within the disc. This precession might cause a deviation in the disc's mid-plane from its initial orientation. For example, Xiang-Gruess & Papaloizou (2013) found significant changes in the form of a disc that was produced by the interaction with larger planet masses, such as visible wrapping in the inner parts, and the difference between the inclination of the inner disc and outer disc is up to 10–20 deg. However, a disc that was initially misaligned with a planet could, over time and multiple precession periods, become aligned with it due to stronger frictional interactions (Xiang-Gruess & Papaloizou 2013). This realignment process may reshape the disc as it unfolds (Mouillet et al. 1997; Kennedy et al. 2012; Pearce & Wyatt 2014; Poblete et al. 2023). So the alignment of planetary systems can serve as an indicator of either primordial conditions or the outcome of subsequent dynamical interactions, contingent upon the system's age. Additionally, high-resolution infrared imaging finds that plenty of discs have non-axisymmetric features in scattered light. We can see that in the closest example TW Hydra, these changes happen on a time-scale of less than 20 yr (Debes et al. 2023), but it is unknown how common these are.

After introducing our methodology in Section 2, in Section 3 our analysis is structured into two distinct sections. In Section 3.1, we employ the inclination values of debris discs to determine the M_{DA} of RV-detected exoplanets that have been identified around HD 10647, HD 115617, HD 69830, GJ 581, HD 22049, and HD 142091. In Section 3.2, we focus on identifying debris disc stars that have not exhibited any prior RV-detected exoplanets. In Section 4 we conclude with a discussion of our findings.

2 METHODOLOGY

Our main source to identify stars with debris discs was the catalogue of circumstellar discs[1] (Traub et al. 2007), complemented by supplementary sources from the literature (Metchev et al. 2005; Maldonado et al. 2010; Eiroa et al. 2013; Tanner et al. 2015; MacGregor et al. 2017; Hengst et al. 2020). Table 1 is our compilation of stars with resolved debris discs, which have been the subject of RV monitoring programmes. Specifically, they were required to possess more than 50 RV data points and exhibit temporal coverage exceeding 1000 d. Where available, disc inclination angles were sourced from the literature. For specific cases, such as HIP 29271 and HIP 85235, where inclination angle data are not in the literature, a direct geometric approach was employed to calculate the inclination angle. It was assumed that the debris discs are circular with zero eccentricity (Mustill & Wyatt 2009) and the difference in the lengths of the major and minor axes arises from the disc inclination, prompting the calculation of inclination angles using the measurements of the major and minor axes from Eiroa et al. (2013). It should be noted that this assumption may not always hold true, as evidenced by cases of warped discs and non-zero eccentricities (Bouvier et al. 1999; Sakai et al. 2019).

The RV data were found from searches across various archives, including the European Southern Observatory (ESO) archive (Romaniello 2022), the Data Analysis Center for Exoplanets (DACE), Exostriker (Trifonov 2019), and the HARPS-RVBank archive (Trifonov et al. 2020). This provided the RV data for the specific stars as listed in Table 1. We extracted the HARPS RV data from the Data Reduction Software (DRS) pipeline within the ESO archive as well as from TERRA pipeline for high activity stars. Importantly, an instrumental update to HARPS in 2015 May led to a discernible jump in the RV data. We utilize the correlation established by Trifonov et al. (2020), between the RV jump and the spectral type of the observed stars in order to make adjustments to the RV data. After acquiring the RV data, we cross-referenced our findings with sources such as Exoplanet Catalogue (NASA) (Akeson et al. 2013) and The Extrasolar Planet Encyclopaedia (2023) to determine whether any exoplanets had been previously identified around these stars using the RV technique.

We conducted our analysis on eight stars known to host RV-detected exoplanets: GJ 581, HD 22049, HD 38858, HD 69830, HD 115617, HD 142091, HD 10700, and HD 10647. For our investigation, we utilized a combined RV data set for these stars. Notably, for some stars − HD 22049, HD 10647, HD 115617, and HD 142091 − we managed to assemble RV data sets larger than those used in previous studies and so provide refined orbital parameters for these stars. Additionally, by assuming the co-planar alignment of both the debris disc and planetary orbits, we calculate the M_{DA} of the RV-detected exoplanets orbiting around them. In the cases of GJ 581 and HD 69830, we were unable to obtain any new RV data beyond what had been previously employed in the literature. For these two stars, we use the available parameters from the literature, and additionally incorporate the inclination angle of the debris disc to deduce M_{DA} for their exoplanets. After this, we conducted a search for exoplanet signals using the RV analysis on the remaining 21 stars, as listed in Table 1.

Our aim is to identify any potential periodic signals indicating the presence of a companion. For this purpose, we plotted Lomb–Scargle (LS) periodograms using DACE. Before constructing the

[1] https://www.circumstellardisks.org/

Table 1. Compilation of stars with resolved debris discs, inclination angle data, more than 50 RV data points, and temporal coverage exceeding 1000 d. We compile stars that have been identified to host exoplanets in existing literature through the use of the RV method. These stars are then sorted in a descending sequence according to their RV_{RMS} values. Likewise, for all remaining stars, we follow a similar approach, arranging them based on their RV_{RMS} values in descending order as well. Column 1 lists the selected stars, Column 2 displays the inclination angle of their debris discs, and Column 3 corresponds to the spectral type of each star. Column 4 indicates the number of previously detected exoplanets around these stars using RV analysis. Column 5 denotes the RV_{RMS} prior to the fitting of planetary models. Column 6 provides references for the inclinations of the debris discs, the spectral classifications of the stars, and the planetary status.

Star	i (deg)	Type	RV-detected exoplanets	RV_{RMS} (m s^{-1})	References
HD 10647	76.7 ± 1.0	F9V	1	11.61	Marmier et al. (2013); Lovell et al. (2021)
GJ 581	50 ± 20	M3V	3	9.38	Lestrade et al. (2012); Trifonov et al. (2018); Reylé et al. (2021)
HD 142091	58 ± 1	K0III	1	7.55	Sato et al. (2012); Baines et al. (2013); Bonsor et al. (2013)
HD 22049	$78.26^{+28.60}_{21.56}$	K2V	1	5.89	Wenger et al. (2000); Greaves et al. (2013); Llop-Sayson et al. (2021)
HD 115617	77 ± 4	G7V	3	4.39	Wenger et al. (2000); Wyatt et al. (2012); Laliotis et al. (2023)
HD 69830	13^{+27}_{-13}	G8V	3	3.78	Payne et al. (2008); Simpson et al. (2010); Tanner et al. (2015)
HD 38858	48	G2V	1	2.59	Kennedy et al. (2015); Flores et al. (2018)
HD 10700	35 ± 10	G8V	4	1.92	Keenan & McNeil (1989); Lawler et al. (2014); Feng et al. (2017)
HD 71155	30	A0V	−	642	Booth et al. (2013)
HD 218396	31 ± 3	A5V	−	610	Gray & Kaye (1999); Pearce et al. (2022)
HD 106906	$84.3 - 85.0$	F5V	−	483	Kalas et al. (2015)
HD 188228	50 ± 20	A0V	−	339	Booth et al. (2013); Pearce et al. (2022)
HD 39060	$85.3^{+0.3}_{-0.2}$	A6V	−	303	Gray et al. (2006); Millar-Blanchaer et al. (2015)
HD 95086	23.3 ± 5.6	A8III	−	229	Moór et al. (2015)
HD 216956	65.6 ± 0.3	A3V	−	227	MacGregor et al. (2017)
HD 172555	14	A7V	−	217	Engler et al. (2018)
HD 197481	89	M1V	−	188	Metchev et al. (2005); Torres et al. (2006)
HD 141943	85	G2V	−	170	Soummer et al. (2014)
HD 202917	68.6 ± 1.5	G7V	−	123	Schneider et al. (2016)
HD 159492	40 ± 14	A5V	−	123	Morales et al. (2016)
HD 206893	40 ± 10	F5V	−	120	Milli et al. (2017); Hinkley et al. (2023)
HD 181327	30.0 ± 0.5	F5V	−	15.74	Schneider et al. (2006); Pearce et al. (2022)
HD 53143	45	G9V	−	15.06	Schneider et al. (2014)
HD 30495	51 ± 10	G2V	−	12.25	Wenger et al. (2000); Maldonado et al. (2010)
HD 202628	57.4 ± 0.4	G2V	−	8.16	Faramaz et al. (2019)
HD 48682	67.5 ± 4.2	G0V	−	5.48	Hengst et al. (2020)
HD 207129	60 ± 3	G2V	−	3.87	Krist et al. (2010)
HIP 29271	56.44 ± 0.23	G5V	−	3.73	Refregier & Douspis (2008); Eiroa et al. (2013)
HIP 85235	66.93 ± 0.04	K0V	−	2.75	Refregier & Douspis (2008); Eiroa et al. (2013)

LS periodogram, we factored in the influence of both stellar jitter and instrumental jitter, focusing solely on this aspect in the initial step of our analysis. Later, we utilized Markov Chain Monte Carlo (MCMC) to fit the jitter as a free parameter. To determine the stellar jitter values, we conducted a review of relevant literature to gather any documented values associated with the star under study. In cases where such values were unavailable in the literature, we employed the methodology outlined in Isaacson & Fischer (2010) to calculate the stellar jitter. Additionally, we considered the reported instrumental precision for various instruments: 2 m s^{-1} for APF (Vogt et al. 2014), 5 m s^{-1} for HAMILTON (Tal-Or et al. 2019), 1 m s^{-1} for HIRES (Tal-Or et al. 2019), 1 m s^{-1} for HARPS (Jenkins et al. 2015), 5 m s^{-1} for CORALIE (Ségransan et al. 2010), and 3 m s^{-1} for UCLES (Jenkins et al. 2015). In our LS periodogram analysis, we considered signals to be significant only if they exhibited a False Alarm Probability (FAP) smaller than 10 per cent (Stempels et al. 2007; VanderPlas 2018b). Our main goal was to differentiate between peaks indicative of exoplanet signals and those arising from stellar activity.

After detecting a potential periodic signal, we examined the rotational period of the star. As suggested by Vanderburg et al. (2016) and Oshagh et al. (2013), periodic signals at the rotational period could potentially arise from stellar modulation, indicating stellar activity rather than an exoplanet signal. We ascertained stellar rotational periods from the literature and where possible, refined these values through the utilization of *TESS* (*Transiting Exoplanet Survey Satellite*) light-curve data (Ricker et al. 2010; Sethi & Martin

2024). Subsequently, after neglecting this signal associated with stellar activity in our periodogram, we proceeded to identify other significant peaks that could potentially indicate exoplanet signals. In certain instances, chromospheric activity was detected at the designated period. Chromospheric activity has the potential to induce both photometric and spectroscopic fluctuations, which within the fitting error resemble exoplanet signals (Martínez-Arnáiz et al. 2010; Rajpaul et al. 2015). Therefore for checking the activity signal we perform an analysis utilizing the S-Index and BIS activity indicators. If we detect the signal in the activity indicators, we classify them as possible activity signals rather than exoplanet signals (Toledo-Padrón et al. 2019; Anna John et al. 2022). Once a period was selected as a potential exoplanet signal, we conducted an analysis to identify aliases of these periods using DACE. Alias peaks emerge due to the periodicity of observations and can surface even in the absence of authentic periodic signals within the data (VanderPlas 2018a). Recognizing these alias peaks as artefacts stemming from the inherent periodic nature of observations (Vogt et al. 2010), we disregard them due to their limited relevance in confirming the presence of exoplanets.

Once a potential exoplanet signal was determined using the periodogram, we utilized DACE to fit a Keplerian model to the RV data, thereby extracting parameters of the planet's orbit (Pepe et al. 2013; Butler et al. 2017). We then use these parameters as priors and conduct MCMC (Díaz et al. 2014, 2016) simulation to determine the orbital parameters, mass, and orbital distance of

the identified planets. For each MCMC simulation, we performed 1 000 000 iterations. Additionally, we also compared these results with the results from Radvel (Fulton et al. 2018) there was no significant change so we used DACE for the RV MCMC analysis. The parameters obtained from the fitting process encompassed the planet's mass M_P, argument of Periastron (ω), orbital period (P), eccentricity (e), time of Periastron Passage (T_P), orbital distance, and velocity amplitude (K). Subsequently, in order to visually validate the model, we employed a phase-folding approach on both the RV data and the model. This procedure proved beneficial in mitigating uncertainties arising from irregularities in data sampling (Grunblatt et al. 2015). We assessed the goodness of fit by conducting a reduced chi-squared test (χ_r^2) (Pepe et al. 2013) and the Bayesian Information Criterion (BIC) for each model and compared it with the BIC of a straight-line model and calculated the ΔBIC.

3 DATA ANALYSIS

Among the stars mentioned in Table 1, HD 38858 exhibited two prominent signals within our data set at periods of 3879.41 and 417.17 d. Further investigation revealed that the 417.17-d signal was an alias of the 3879.14-d signal, likely arising due to a 1-yr periodicity. When fitting a Keplerian model to the 3879.14-d signal, an orbit with a high eccentricity ($e \approx 0.55$) was suggested. However, upon closer examination, the 3879.41-d signal was identified as chromospheric activity according to Flores et al. (2018), rather than being indicative of an exoplanet. In our analysis, we also examined the S-Index indicator and identified a peak near the 3879-d period, consistent with the findings of Flores et al. (2018), who similarly observed the signal in both the S-Index and I_α indicators and confirmed it as indicative of chromosphere activity.

HD 10700 has undergone extensive monitoring by HARPS. While numerous planet candidates have been identified, there remains a lack of consensus among various analyses (Tuomi et al. 2013; Feng et al. 2017; Coffinet et al. 2019). In our investigation, we integrated a total of 10 603 RV data points acquired from the HARPS instrument, along with an additional 803 data points from HIRES. However, this data set spans a considerable duration of 6350 d, and the periodic signals detected within it are relatively weak. Moreover, Allart et al. (2022) found that the RV signature of micro-tellurics in HD 10700 is up to 58 cm s^{-1}, similar in magnitude to the RV amplitudes of the putative exoplanets. They caution that interpreting small-amplitude exoplanet signals requires consideration of micro-tellurics. However, such analysis is beyond the scope of this study. Therefore, for the purpose of this work, HD 10700 is considered a star without RV-detected planetary companions.

Subsequently, we observed that the stars HD 39060, HD 172555, HD 106906, HD 141943, HD 202917, HD 71155, HD 95086, HD 159492, HD 197481, HD 206893, HD 216956, HD 218396, and HD 188228 stand out due to their significantly elevated RV_{RMS} values of greater than 100. We note that for these stars, the DRS pipeline produces significantly larger RMS residuals and so we also used TERRA for data reduction, following the methodology outlined by Anglada-Escudé & Butler (2012). Upon comparing the resulting RV_{RMS} value with the literature, we observed that the RV_{RMS} of HD 188228 was 339 m s^{-1}, similar to the value of 319 m s^{-1} found by the work of Grandjean et al. (2020) specifically focused on hot stars. Therefore, we proceeded with the RV_{RMS} based on TERRA reduction. Upon conducting an RV analysis of these stars, we did not identify any significant periodic signal in 13 out of 14 stars. It is evident that some of the stars with high values of RV_{RMS} already harbour directly imaged exoplanets. However, planets around five of the stars exhibit long orbital periods. Due to the absence of RV data covering such extended temporal ranges, we are unable to detect these planets in our data. However, for HD 206893, Hinkley et al. (2023) detected the planet using the direct imaging method and utilized RV data to calculate the orbital parameters of HD 206893 c. We try to mimic the signal identified by Hinkley et al. (2023), considering the RV data alone and using a jitter of 40 m s^{-1} appropriate for a young star. We note that the detected planet has an orbital period of 5.7 yr which is longer than the 5.2 yr coverage of the RV data. Notably, although there are 132 RV measurements, the majority are clustered within a few nights, providing effectively only 11 epochs to constrain the signal. Our fit provides a χ_r^2 value of 4.09 and ΔBIC value of 616.77 for the orbital solution of HD 206 892 c which does not provide substantial support for its detection.

We detect a periodic signal around HD 106906 with a period of 49.22±5.04 using TERRA RV data which is consistent with Lagrange et al. (2016). We note that Gaia DR3 classifies HD 106906 as a single star based on its RUWE value of 0.93 (Vallenari et al. 2023) but it should be noted that based on fig. 9 of Castro-Ginard et al. (2024) that *Gaia* has little sensitivity to short-period near equal mass binaries. However, Lagrange et al. found that HD 106 906 is an equal-mass spectroscopic binary system, consisting of two young F-type stars with nearly identical masses. The combined mass of these stars is approximately 2.6 M$_\odot$, and they orbit each other at a distance of 0.36±0.002 AU (Lagrange et al. 2016; Rodet et al. 2017; De Rosa & Kalas 2019). The TERRA pipeline assumes that HD 106 906 is a single star (SB1), which provides one set of RV measurements. However, HD 106906 is actually a spectroscopic binary system (SB2), e.g. fig. 1 of De Rosa & Kalas (2019) making it necessary to extract two sets of RVs − one for each star. Since this data set would require a different data analysis approach to account for its binarity we consider this system as being beyond the scope of this paper. With additional radial velocity epochs as well as DR4 *Gaia* astrometry HD 106906 should make a promising candidate for a full orbit fit (Gallenne et al. 2023). We note that we also examined the *TESS* data and detected a consistent rotational period of 1.6 d across *TESS* sectors 11, 37, and 64. This period aligns with the periodic signal found by Green et al. (2023).

Finally, six stars meeting our established criteria and displaying lower RV_{RMS} values showed no RV-detected exoplanets. HD 48682, characterized by 92 RV data points – 50 sourced from HIRES and 42 from HARPS; HIP 85235, represented by a collection of RV data points – 17 from ELODIE and 66 from HIRES; HD 30495, featuring a compilation of 134 RV data points obtained from HARPS; HD 181327, showing 63 HARPS RV data points; HIP 29271, comprising an assemblage of 237 HARPS data points; and HD 53143, consisting of 90 HARPS RV data points.

We now move forward to investigate the remaining eight stars. Among these, exoplanets have previously been detected using the RV method in six stars, while the remaining two stars have shown no exoplanet detections through the RV method. The stellar parameters employed to compute the attributes of potential exoplanets are outlined in Table 2.

3.1 Analysis of stars with detected exoplanets using the radial velocity method

In this section, we present HD 10647, HD 115617, HD 69830, HD 142091, HD 22049, and GJ 581. Among these six target stars, we managed to employ an expanded data set and revise the orbital parameters for four of them: HD 10647, HD 115617, HD 22049, and HD 142091.

Table 2. Stellar parameters used to compute candidate exoplanet parameters around our target stars and also employed for statistical analysis. 1. (Vallenari et al. [2023]), 2. (Marmier et al. [2013]), 3. (Perrin et al. [1988]), 4. (Von Braun et al. [2014]), 5. (Bean et al. [2006]), 6. (Pineda et al. [2021]), 7. (Suárez Mascareño et al. [2017]), 8. (Tanner et al. [2015]), 9. (Laliotis et al. [2023]), 10. (Simpson et al. [2010]), 11. (Marshall et al. [2011]), 12. (Holmberg et al. [2007]), 13. (Pasinetti-Fracassini et al. [2001]), 14. (Gáspár et al. [2016]), 15. This Study, 16. (Mamajek & Hillenbrand [2008]), 17. The Extrasolar Planet Encyclopaedia ([2023]), 18. (Krist et al. [2012]), 19. (Favata et al. [1997]), 20. (White et al. [2018]), 21. (Bonsor et al. [2013]), 22.(Benedict et al. [2006]), 23. (Demory et al. [2009]), 24. (Roettenbacher et al. [2021]), 25. (Santos et al. [2004]), 26. (Van Leeuwen [2007]).

Stars	Mass ($M_\odot$)	Radius ($R_\odot$)	P_{Rot} (d)	[Fe/H] (dex)	Age (Gyr)	References
HD 10647	1.11 ± 0.02	1.10 ± 0.02	10 ± 3	0.00 ± 0.01	1.4 ± 0.9	1, 2, 15
HD 115617	0.93	0.987 ± 0.005	29	-0.02	6.1 to 6.6	1, 3, 4, 16
GJ 581	0.31 ± 0.01	0.310 ± 0.008	132.5 ± 6.3	-0.33 ± 0.12	8^{+3}_{-1}	1, 5, 6, 7, 17
HD 69830	0.89 ± 0.03	0.905 ± 0.019	35.1 ± 0.8	-0.04 ± 0.03	10.6 ± 4.0	1, 8, 9, 10
HD 142091	1.32 ± 0.10	4.77 ± 0.07	$-$	0.13 ± 0.03	2.5	1, 20, 21
HD 207129	$0.97^{+0.07}_{-0.05}$	1.0	12.6	-0.15	$3.8^{+3.6}_{-2.5}$	1, 11, 12, 13
HD 202628	1.068 ± 0.038	0.951 ± 0.013	14.91 ± 0.03	0.00 ± 0.06	2.3 ± 1.0	1, 14, 15, 18, 19
HD 22049	0.82 ± 0.02	0.735 ± 0.005	11.4	-0.13 ± 0.04	0.4 to 0.8	22, 23, 24, 25, 26

3.1.1 HD 10647

HD 10647, classified as an F9V star (Lovell et al. [2021]), exhibits a surrounding disc that was initially detected by the IRAS space-based telescope. The detection was based on the observation of an excess of infrared radiation (Stencel & Backman [1991]). Extensive investigations by Lovell et al. ([2021]) and Liseau et al. ([2008]) have revealed that the disc possesses a high inclination, indicating an asymmetrical structure that extends predominantly in the northward direction. During the XIX IAP Colloquium Extrasolar exoplanets: Today and Tomorrow, an exoplanet named 10647b was first identified around HD 10647 by Michael Mayor in 2003. The existence of this planet was subsequently confirmed by Butler et al. ([2006]). In 2013, Marmier et al. ([2013]) conducted a study on this planet, utilizing CORALIE RV data for their analysis.

Our investigation commenced with an analysis of the stellar rotational period of HD 10647. Mamajek & Hillenbrand ([2008]) employed the stellar modulation technique and suggested a rotational period of 10 ± 3 d. In addition to this, we utilized *TESS* data to independently determine the rotational period. Our findings align with Mamajek & Hillenbrand ([2008]) so we adopt their value. For our RV analysis, we analysed 330 RV points acquired from multiple instruments, including HARPS, CORALIE98DRS-3.3 (COR98DRS-3.3), University College London Echelle Spectrograph (UCLES), and CORALIE07DRS-3.4 (COR07DRS-3.4). These RV measurements spanned the period from 1998 January 17, to 2020 January 17. We took into account the effect of RV jitter, Butler et al. ([2006]) calculated the RV jitter for HD 10647 to be $4.2\,\mathrm{m\,s^{-1}}$. Additionally, we considered the error values in the RV measurements for each instrument. The LS periodogram for our RV data reveals a prominent peak at a period of 964.14 d, as depicted in Fig. 1(a). We applied a one-Keplerian model to determine priors and perform MCMC to calculate the orbital parameters. Specifically, a single-planet Keplerian model was employed to analyse the RV data set, as depicted in Fig. 1(b), since no other notable peaks were observable. The optimal solution yielded a $\chi_r^2 = 2.31$ and a ΔBIC value of 1016. The RV_{RMS} for the best fit was determined to be $7.84\,\mathrm{m\,s^{-1}}$.

In conclusion, we present a phase-folded Keplerian model with a period of 992.10 ± 1.45 d, visually confirming the observed periodic variations. Fig. 1(c) illustrates the phase-folded diagram. We employed a more extensive data set of RV data points in comparison to Marmier et al. ([2013]) and Butler et al. ([2006]), thereby facilitating the refinement of the orbital parameters. Additionally, we incorporated the inclination angle value of the debris disc around HD 10647 as mentioned in Table 1, enabling the determination of M_{DA}

of HD 10647b. All orbital parameters for HD 10647b, calculated within this study and compared to those from the previous study by Marmier et al. ([2013]), have been detailed in Table 3.

3.1.2 HD 115617

The G6V star HD 115617 commonly referred to as 61 Vir has garnered significant attention in recent years (Gray et al. [2003]). The *Spitzer space telescope* revealed the presence of a debris disc surrounding the star, manifesting as an infrared radiation excess at a wavelength of 160 μm (Wyatt et al. [2012]). In 2009 December, Vogt et al. ([2009]) provided the discovery of three exoplanets orbiting HD 115617, designated as 61 Vir b, 61 Vir c, and 61 Vir d. Initially, the existence of 61 Vir b and 61 Vir c was confirmed based on HARPS data in 2012 (Wyatt et al. [2012]). However, at that time, the exoplanet signals associated with 61 Vir d remained unconfirmed. In 2021, Rosenthal et al. ([2021]) identified the signal as a yearly alias, suggesting it to be a false positive. Contrarily, a recent study conducted by Laliotis et al. ([2023]) proposed that the signals attributed to 61 Vir d do indeed represent exoplanet signals.

Baliunas et al. ([1995]) reported an average rotation period of 29 d based on analysis of the Mt. Wilson survey data. We also generated a *TESS* LC for HD 115617 and then analysed it. However, the LC exhibited no discernible evidence of a periodic signal, offering no assistance in determining the rotational period of the star. Consequently, we use the Baliunas et al. ([1995]) value for the rotational period of the star. Our analysis incorporated a total of 3124 RV measurements obtained from various instruments, covering the period from 1991 April 30, to 2021 August 6. Specifically, we collected 179 RVs from APF, 171 RVs from HAMILTONPub-2014, 173 RVs from HAMILTONPub-2021, 602 RVs from HIRESPub-2021, 80 RVs from HIRESPub-2010, 520 RVs from HIRESPub-2017, 1273 RVs from HARPS, and 126 RVs from UCLESPub-2010. When considering the RV measurements, we accounted for the RV jitter. Vogt et al. ([2009]) showed a stellar jitter of $1.5\,\mathrm{m\,s^{-1}}$ for this star with the instrumental precision. Using these RV measurements, we generated LS periodograms for the merged RVs. To ensure the accuracy of our analysis, we disregarded any peaks at the stellar rotation period that could be attributed to stellar activity, focusing only on exoplanet signals. We identify three significant peaks corresponding to planetary systems. No other significant peaks were found apart from these three periods. A three-planet Keplerian model, aligned with the respective periods, was employed to ascertain the priors and perform MCMC. The goodness of our three-planet
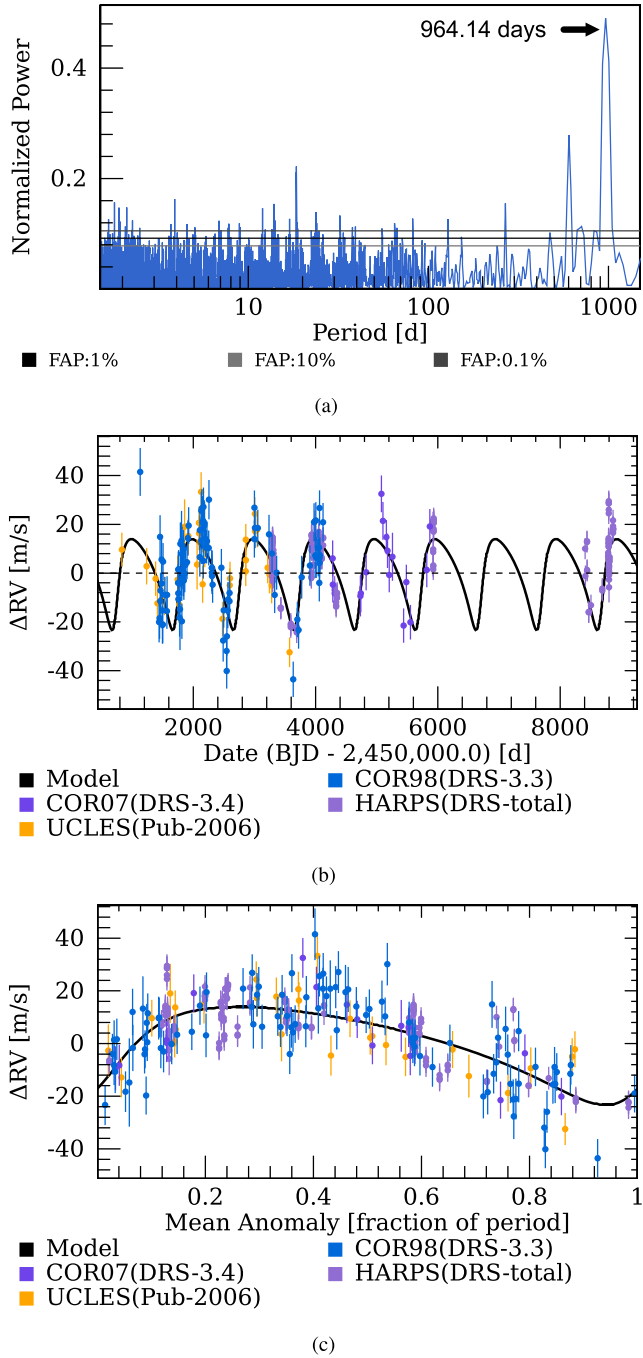
(a)

(b)

(c)

Figure 1. (a) LS periodogram of the RV data for HD 10647, exhibiting marked FAP values represented by three horizontal lines. Notably, a highly significant peak at 964.14 d is observed, signifying a periodic signal. (b) Doppler measurements of HD 10647 obtained from CORALIES, HARPS, and UCLES are presented as a scatter plot. The best-fitting Keplerian model at 992.1 ± 1.4 d is superimposed on the data, illustrated by the black curve. (c) RV data and the one-planet Keplerian model phase-folded at 992.1 d. The phased data and our model demonstrate an excellent fit, confirming the presence of the detected periodic signal.

Table 3. Orbital parameters of HD 10647b.

Parameter	Marmier et al. (2013)	This study
P(d)	989.2 ± 8.1	991.90 ± 1.45
e	0.15 ± 0.08	0.37 ± 0.03
ω(deg)	212 ± 39	225.3 ± 4.3
K(m s^{-1})	18.1 ± 1.7	18.44 ± 0.91
T_P(JD)	2453654 ± 99	2454700.68 ± 10.82
$M_P\sin i$ ($M_{\rm Jup}$)	0.94 ± 0.08	0.90 ± 0.04
$M_{\rm DA}$ ($M_{\rm Jup}$)	–	1.07 ± 0.05
Orbital distance (AU)	2.015 ± 0.011	2.02 ± 0.01

Keplerian MCMC model was calculated by a χ_r^2 value of 1.44 and ΔBIC of 8073.85. The $RV_{\rm RMS}$ for the best fit was 2.56 m s^{-1}.

We have compiled a comparative table detailing our observations, as outlined in Table 4. It is noteworthy that Vogt et al. (2009) employed 206 individual measurements from HIRES and AAT spanning a 16-yr time-series, while Laliotis et al. (2023) utilized a total of 1653 RV measurements from diverse instruments, including HIRES, UCLES, and HARPS, gathered between 2004 and 2020. In our investigation, we combined data sets from HIRES, HARPS, HAMILTON, and UCLES, encompassing a total of 3124 measurements taken between 1991 April 30, and 2021 August 6. Our outcomes demonstrate agreement with the prior findings, as all parameters fell within the uncertainty range reported by Vogt et al. (2009) and Laliotis et al. (2023). However, due to the larger RV data set at our disposal, we provide updated orbital parameters for these exoplanets. Additionally, by incorporating the inclination angle value from Table 1, we calculate $M_{\rm DA}$ of the exoplanets.

3.1.3 HD 142091

Bonsor et al. (2013) reported the detection of a debris disc surrounding HD 142091 (κ Coronae Borealis). Additionally, Johnson et al. (2008) identified an exoplanet orbiting this star using RV analysis. Subsequently, Sato et al. (2012) leveraged 96 RV data points obtained from the HAMILTON spectrograph (Spronck et al. 2013) to corroborate the presence of this exoplanet. Finally, we integrate 416 RV points from HIRES, resulting in a compilation of 512 RV data points.

For our observation, we utilized RV data spanning from 2004 April 20, to 2014 August 26. We commenced our observation by investigating the stellar jitter of this star, which had been reported as 2.84 m s^{-1} by Luhn et al. (2020). Additionally, we took into account an instrumental precision and generated an LS periodogram for our RV data, revealing a significant peak at 1257.95 d. We also attempted to determine the rotational period of this star from existing literature and *TESS* data however no results were obtained. Given that we identified only one significant signal at 1257.95 d — unusually too long for a rotational period of a K-type star — proceeded with our investigation. We employed a one-planet Keplerian model at the designated period and determine priors for the MCMC simulations. The fitting yielded a result, exhibiting a χ_r^2 value of 0.69 and a ΔBIC value of 3528.96. The $RV_{\rm RMS}$ for the best fit was 2.81 m s^{-1}. Furthermore, we present our findings alongside an analysis conducted by Baines et al. (2013), who also incorporated the inclination angle of the disc to ascertain $M_{\rm DA}$ of the identified planet. In line with their methodology, we provide an updated parameter assessment, utilizing an expanded data set derived from earlier studies. The complete set of parameters is tabulated in Table 5.

Table 4. Orbital parameter of exoplanets detected around HD 115617.

Planet	Parameter	Vogt et al. (2009)	Laliotis et al. (2023)	This study
	P (d)	4.2150 ± 0.0006	4.21498 ± 0.00014	4.2150 ± 0.0001
	e	0.12 ± 0.11	0.033 ± 0.029	0.11 ± 0.03
	ω(deg)	105 ± 54	–	121.4 ± 29.2
61 Vir b	K(m s^{-1})	2.12 ± 0.23	2.47 ± 0.11	2.56 ± 0.05
	T_P(rjd)	53369.166	–	55501.33 ± 0.13
	$M_P \sin i$ ($M_{\rm Earth}$)	5.1 ± 0.5	$5.98^{+0.30}_{-0.29}$	6.11 ± 0.24
	$M_{\rm DA}$ ($M_{\rm Jup}$)	–	–	0.197 ± 0.001
	Orbital distance (AU)	0.050201 ± 0.000005	–	0.050 ± 0.001
	P (d)	38.021 ± 0.034	38.079 ± 0.008	38.073 ± 0.003
	e	0.14 ± 0.06	0.026 ± 0.023	0.07 ± 0.01
	ω(degree)	341 ± 38	–	327 ± 14
61 Vir c	K(m s^{-1})	3.62 ± 0.23	3.56 ± 0.12	3.87 ± 0.06
	T_P(rjd)	53369.166	–	55487.45 ± 1.47
	$M_P \sin i$ ($M_{\rm Earth}$)	24.0 ± 2.2	17.94 ± 0.73	19.33 ± 0.70
	$M_{\rm DA}$ ($M_{\rm Jup}$)	–	–	0.062 ± 0.002
	Orbital distance (AU)	0.2175 ± 0.0001	–	0.216 ± 0.004
	P(d)	123.01 ± 0.55	123.2 ± 0.2	123.12 ± 0.08
	e	0.35 ± 0.09	0.15 ± 0.11	0.12 ± 0.03
	ω(deg)	314 ± 20	–	309 ± 4
61 Vir d	K(m s^{-1})	3.25 ± 0.39	1.47 ± 0.17	1.66 ± 0.06
	T_P(rjd)	53369.166	–	55405.098 ± 7.736
	$M_P \sin i$ ($M_{\rm Earth}$)	18.2 ± 1.1	$10.82^{+1.23}_{-1.03}$	12.24 ± 0.59
	$M_{\rm DA}$ ($M_{\rm Jup}$)	–	–	0.040 ± 0.002
	Orbital distance (AU)	0.476 ± 0.001	–	0.47 ± 0.01

Table 5. Orbital parameters of HD 142091 b.

Parameter	Baines et al. (2013)	This study
P (d)	1300 ± 15	1265.96 ± 4.72
e	0.125 ± 0.049	0.128 ± 0.034
ω(deg)	–	181.76 ± 13.95
K (m s^{-1})	27.3 ± 1.3	25.74 ± 0.77
T_P(rjd)	–	54819.83 ± 589.60
$M_P \sin i$ ($M_{\rm Jup}$)	1.88 ± 0.09	1.63 ± 0.01
$M_{\rm DA}$ ($M_{\rm Jup}$)	2.17	1.92 ± 0.01
Orbital distance (AU)	2.8 ± 0.1	2.51 ± 0.06

3.1.4 HD 22049

HD 22049, also known as Epsilon Eridani, was identified by the Infrared Astronomical Satellite (IRAS) (Aumann 1985) as having an infrared excess indicating the presence of circumstellar dust. Subsequent observations conducted with the James Clerk Maxwell Telescope (JCMT) at a wavelength of 850 μm unveiled an extended flux of radiation extending to an angular radius of 35 arcsec around Epsilon Eridani, marking the first resolution of the debris disc. Subsequent higher resolution imaging, employing ALMA, pinpointed the belt's location at 70 au from the star, with a width of merely 11 au (Booth et al. 2017, 2023). Designated as Epsilon Eridani b, the existence of this planet was officially announced in 2000 (Hatzes et al. 2000), but its discovery stirred controversy over the ensuing two decades. In a 2008 study, the detection was labelled as 'tentative,' describing the proposed planet as 'long suspected but still unconfirmed' (Backman et al. 2008). Despite skepticism, numerous astronomers considered the evidence sufficiently compelling to confirm the discovery (Heinze et al. 2008; Brogi et al. 2009; Reidemeister et al. 2011). However, doubts resurfaced in 2013 when a search program at La Silla Observatory failed to confirm the planet's existence (Zechmeister et al. 2013). Subsequent investigations since 2018 gradually reaffirmed the planet's presence

through a combination of RV and astrometry (Llop-Sayson et al. 2021; Makarov et al. 2021). In our analysis, we utilized a total of 2192 RV data points from instruments such as HARPS, HIRES, HAMILTON, and APF, and during this examination, we successfully detected Epsilon Eridani b.

We analysed RV data spanning from 1987 September to 2020 February. As the available literature lacked information on the stellar jitter, we computed the RV jitter for this star following the methodology outlined in Isaacson & Fischer (2010). We utilized values from Jenkins et al. (2006), resulting in a calculated stellar jitter of 3.56 m s^{-1}. Additionally, we considered instrumental precision and generated an LS periodogram for our RV data, revealing a highly significant peak at 2774.41 d. Furthermore, we took into account the rotational period of the star, determined to be 11.4 d based on findings by Roettenbacher et al. (2021). To further investigate the potential exoplanet signal, we employed a one-planet Keplerian model at the identified period and determined priors for MCMC simulation. The fitting process resulted in an outcome, with a χ^2_r value of 2.80 and a ΔBIC value of 4870.1. $RV_{\rm RMS}$ for the best fit was 7.59 m s^{-1}. Moreover, we present our findings alongside an analysis conducted by Feng et al. (2023), who used orbital inclination value derived using astrometric data and calculated the mass of the planet. A detailed summary of all parameters is presented in Table 6.

3.1.5 HD 69830

HD 69830, a G8V star, has been the subject of significant astronomical investigation. The presence of a narrow ring of warm debris encircling the star was initially detected by the *Spitzer Space Telescope* in 2005 (Beichman et al. 2005). Subsequent exploration led to the confirmation of three exoplanets with minimum masses similar to those of Neptune. These exoplanets are all situated within the orbit of the debris ring. In our study, we utilized 648 RVs from the HARPS instrument and 439 RVs from HIRES, resulting in

Table 6. Orbital parameters of HD 22049b.

Parameter	Feng et al. (2023)	This study
P (d)	$2688.60^{+16.17}_{-16.51}$	2806.04 ± 5.55
e	0.26 ± 0.04	0.16 ± 0.01
ω(deg)	224.37 ± 5.87	225.3 ± 4.3
K(m s^{-1})	9.98 ± 0.43	11.37 ± 0.20
T_P(RJD)	44411.54 ± 76.60	52785.68 ± 61.09
$M_P\sin i$ (M_{Jup})	–	0.68 ± 0.03
M_P (M_{Jup})	$0.76^{+0.14}_{-0.11}$	–
M_{DA} (M_{Jup})	–	0.70 ± 0.03
Orbital distance (AU)	3.53 ± 0.06	3.64 ± 0.06

Table 7. Orbital parameter of exoplanets detected around HD 69830. The source of the values in the table (Ref) is given in the final column: 1.(Laliotis et al. 2023), 2. This study.

Planet	Parameter	Best fit	Ref
	P(d)	8.66897 ± 0.00028	1
	e	0.128 ± 0.028	1
HD 69830 b	K(m s^{-1})	3.4 ± 0.1	1
	$M_P\sin i$ (M_{Earth})	$10.1^{+0.38}_{-0.37}$	1
	M_{DA} (M_{Jup})	$0.14^{+1.75}_{-0.34}$	2
	Orbital distance (AU)	0.079 ± 0.001	2
	P(d)	31.6158 ± 0.0051	1
	e	0.03 ± 0.03	1
HD 69830 c	K (m s^{-1})	2.6 ± 0.1	1
	$M_P\sin i$ (M_{Earth})	$12.09^{+0.55}_{-0.54}$	1
	M_{DA} (M_{Jup})	$0.17^{+2.12}_{-0.11}$	2
	Orbital distance (AU)	0.188 ± 0.001	2
	P (d)	201.4 ± 0.4	1
	e	0.08 ± 0.07	1
HD 69830 d	K (m s^{-1})	1.5 ± 0.1	1
	$M_P\sin i$ (M_{Earth})	$12.26^{+0.89}_{-0.88}$	1
	M_{DA} (M_{Jup})	$0.17^{+2.17}_{-0.11}$	2
	Orbital distance (AU)	0.644 ± 0.001	2

Table 8. Orbital parameters of exoplanets detected around GJ 581. 1. (Trifonov et al. 2018), 2. This study.

Planet	Parameter	Best fit	Ref
	P (d)	5.368 ± 0.001	1
	e	$0.022^{+0.027}_{-0.005}$	1
	ω(deg)	$118.3^{+27.4}_{-22.9}$	1
Gliese 581 b	K (m s^{-1})	$12.35^{+0.18}_{-0.20}$	1
	M (deg)	$163.4^{+22.9}_{-23.9}$	1
	$M_P\sin i$ (M_{Earth})	$15.20^{+0.22}_{-0.27}$	1
	M_{DA} (M_{Jup})	0.048 ± 0.001	2
	Orbital distance (AU)	0.041 ± 0.001	1
	P(d)	$12.919^{+0.003}_{-0.002}$	1
	e	$0.087^{+0.150}_{-0.016}$	1
	ω(deg)	$148.7^{+71.5}_{-33.0}$	1
Gliese 581 c	K(m s^{-1})	$3.28^{+0.22}_{-0.12}$	1
	M (deg)	$218.0^{+37.3}_{-68.4}$	1
	$M_P\sin i$ (M_{Earth})	$5.652^{+0.386}_{-0.239}$	1
	M_{DA} (M_{Jup})	0.018 ± 0.001	2
	Orbital distance (AU)	0.074 ± 0.001	1
	P(d)	$3.153^{+0.001}_{-0.006}$	1
	e	$0.125^{+0.078}_{-0.015}$	1
	ω(deg)	$77.4^{+23.0}_{-43.6}$	1
Gliese 581 e	K(m s^{-1})	$1.55^{+0.22}_{-0.13}$	1
	M (deg)	$203.7^{+56.6}_{-21.4}$	1
	$M_P\sin i$ (M_{Earth})	$1.657^{+0.240}_{-0.161}$	1
	M_{DA} (M_{Jup})	0.005 ± 0.001	2
	Orbital distance (AU)	0.029 ± 0.001	1

presence of three exoplanet signals, consistent with the discoveries of Trifonov et al. (2018). Given the absence of updated RV data, we reference Trifonov et al. (2018) in Table 8. Furthermore, we incorporated the debris disc inclination angle value from Table 1 and determined M_{DA} of the detected exoplanets.

3.2 Analysis of stars without detected exoplanets using the radial velocity method

In the subsequent sections, we provide a detailed analysis of two of these stars, namely HD 207129 and HD 202628, elucidating their RV characteristics and potential for hosting undiscovered companions.

3.2.1 HD 207129

HD 207129 is a G2V star and has been the subject of study using the Advanced Camera for Surveys (ACS) instrument on the *Hubble Space Telescope*. Notably, imaging of a debris disc around HD 207129 has been accomplished both in visible light using the ACS instrument and in the infrared (70 µm) using the MIPS instrument on the *Spitzer Space Telescope* (Krist et al. 2010).

Before our investigation, no exoplanets had been detected in close proximity to HD 207129. To conduct our analysis, we incorporated 482 RV points from HARPS with a stellar jitter value of 1.76 m s^{-1} (Hojjatpanah et al. 2020). Considering the instrumental precision, we focused on determining the rotational period of HD 207129, which was found to be 12.6 d (Marshall et al. 2011). Additionally, we utilized *TESS* data to search for the rotational period but did not find any periodic signal, so we proceeded with the rotational period value from the literature for our analysis. In our investigation of periodic
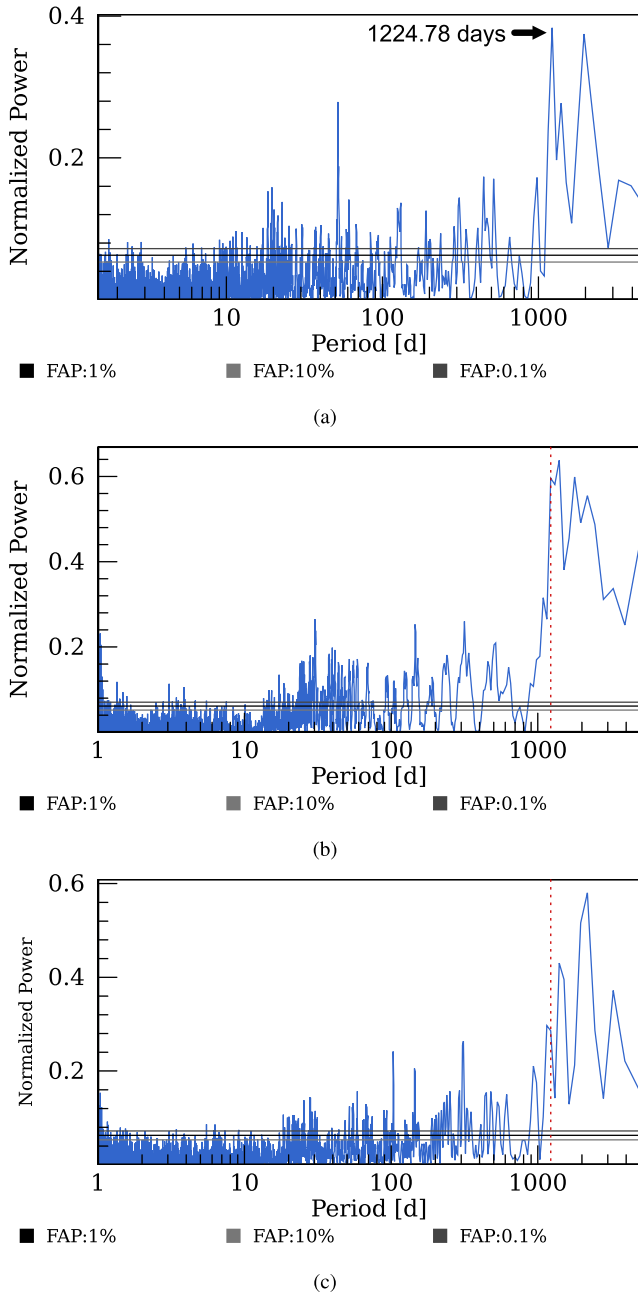
in a total of 1087 RVs data points. However, Laliotis et al. (2023) employed a more extensive data set, consisting of 1589 RV data points, which represents an update to our analysis. We also utilize the disc inclination angle to derive the M_{DA} of the planet. Additionally, we determined the orbital distance using the data set available to us, and we have summarized the relevant parameters in Table 7.

3.1.6 GJ 581

GJ 581 is categorized as an M3V star with a mass roughly one-third that of the Sun (Reylé et al. 2021). The presence of a debris disc around GJ 581 was noted within the DEBRIS program conducted on the *Herschel Space Observatory* (Lestrade et al. 2012). The initial planet in orbit around GJ 581 was discovered in 2005 August (Bonfils et al. 2005). Following this discovery, the same group identified two additional exoplanets, Gliese 581c and Gliese 581d (Udry et al. 2007). Another planet, Gliese 581e, was announced on 2009 April 21 (Mayor et al. 2009b). Subsequent findings introduced Gliese 581g and Gliese 581f as two more exoplanets orbiting this star (Vogt et al. 2010). Although later investigations indicated that Gliese 581f was more likely associated with the stellar activity cycle (Ballard et al. 2013; Robertson et al. 2013; Trifonov et al. 2018) argued for the existence of three exoplanets encircling GJ 581 — specifically Gliese 581b, Gliese 581c, and Gliese 581e. Our analysis also confirmed the

Figure 2. Panel a: LS Periodogram of HARPS RV data for HD 207129, emphasizing the most prominent peak at 1224.78 d (indicated by an arrow). Panel b: LS Periodogram for the S-Index Indicator of HD 207129, with the dotted line representing the 1224.78 d period. Panel c: LS Periodogram for the BIS Indicator, with the dotted line indicating the 1224.78 d period.

signals in the RV data, we identified several significant peaks with FAP better than 0.1 per cent as shown in Fig. 2(a). To explore potential exoplanet signals further, we performed a Keplerian fit to the three most significant peaks observed at periods of 51.57, 1224.78, and 1959.65 d. A single-planet Keplerian model was applied to all three peaks, but we observed highly eccentric orbits ($e \geq 0.5$), except for the most significant peak at 1224.78 d, leading us to consider it a candidate planetary peak. In order to confirm whether the observed signal indicates a planetary presence or merely activity, we conducted an analysis using the S-Index and BIS indicators. Subsequently, we plotted LS periodograms for both indicators, as depicted in Figs 2(b)

and (c), respectively. The periodograms for both the S-Index and BIS indicators reveal prominent peaks occurring at 1224.78 d. The normalized powers associated with these peaks are 0.6 for the S-Index and 0.29 for BIS. Upon comparing these power values with the normalized power of the LS periodogram in Fig. 2(a), which stands at 0.38, it becomes evident that the S-Index activity signal significantly surpasses the RV signal. Therefore, based on this comparison, we conclude that the observed signal is more likely attributable to a possible activity rather than an exoplanet signal.

3.2.2 HD 202628

HD 202628 is a G2V star similar to that of the Sun (Faramaz et al. 2019). In 2010, the *Spitzer space telescope* detected infrared excess from a circumstellar disc around this star. On analysing the disc, Faramaz et al. (2019) saw a sharply defined inner edge of the disc at a distance of 150 AU, and Nesvold & Kuchner (2014) showed that an exoplanet is responsible for this sharp inner edge.

No literature regarding the rotational period of the star HD 202628 was found. We utilized data from *TESS* to determine the stellar rotational period of HD 202628. For our analysis, we extracted *TESS* data using the SPOC pipeline, as suggested by Martins et al. (2020). The light curves (LCs) of each *TESS* sector were then de-trended with third-order polynomial fits. This step serves as a high-pass filter, suppressing long-term trends typically associated with instrumental systematics. Subsequently, we performed the removal of outliers by excluding any flux measurement greater than 3.5 times the standard deviation of the de-trended LCs. Upon extracting the *TESS* data, observations were available in two sectors, namely Sector 1 and Sector 29. Our intention was to combine these two sectors to form a long-term series. However, inspected of the individual sectors shows the variation observed in sector 1, as shown in Fig. 3(a), was absent in sector 29. In sector 29, the light curve appeared almost linear. The reason for this discrepancy is attributed to the absence of starspots, not unexpected given the approximately 2-yr time difference between the observations in different sectors puts a Sun-like star in a different phase of its activity cycle. Consequently, for our analysis, we focus on *TESS* Sector 1 data. Here a rotational period of 14.91 d was detected, accompanied by a low FAP of less than 0.01 per cent. Subsequently, we phase-folded the data set using the identified period of 14.91 d, as demonstrated in Fig. 3(b). This phase-folded representation exhibited a distinct dip, providing evidence for a stellar rotational period. We employed an LS periodogram on the LC data, depicted in Fig. 3(c). The LS periodogram indicated a peak at a period of 14.91 ± 0.03 d, which we identify as the rotational period of the star.

Our RV analysis involved examining 179 measurements obtained from HARPS. As the literature lacked information regarding the stellar jitter, we calculated the RV jitter for this star following the methodology mentioned in Isaacson & Fischer (2010) and utilizing the S_{HK} values from Jenkins et al. (2006), resulting in a stellar jitter of 4.16 m s^{-1}. We also considered instrumental errors, to validate the detected stellar rotational period of 14.91 ± 0.03 d, we constructed an LS periodogram for the RV data, revealing a significant peak with a FAP better than 0.1 per cent at a period of 15.08 d, as depicted in Fig. 4(a). This finding reaffirmed the accuracy of the identified stellar rotational period. We further explored potential exoplanet signals, observing a notable peak at 572.182 d in Fig. 4(a). Subsequently, we sought the presence of the 572.182-d signal in both the S-Index and BIS indicators. We identify a signal in the S-index, as illustrated by dotted red line in Fig. 4(b) though no signal is evidence in the BIS
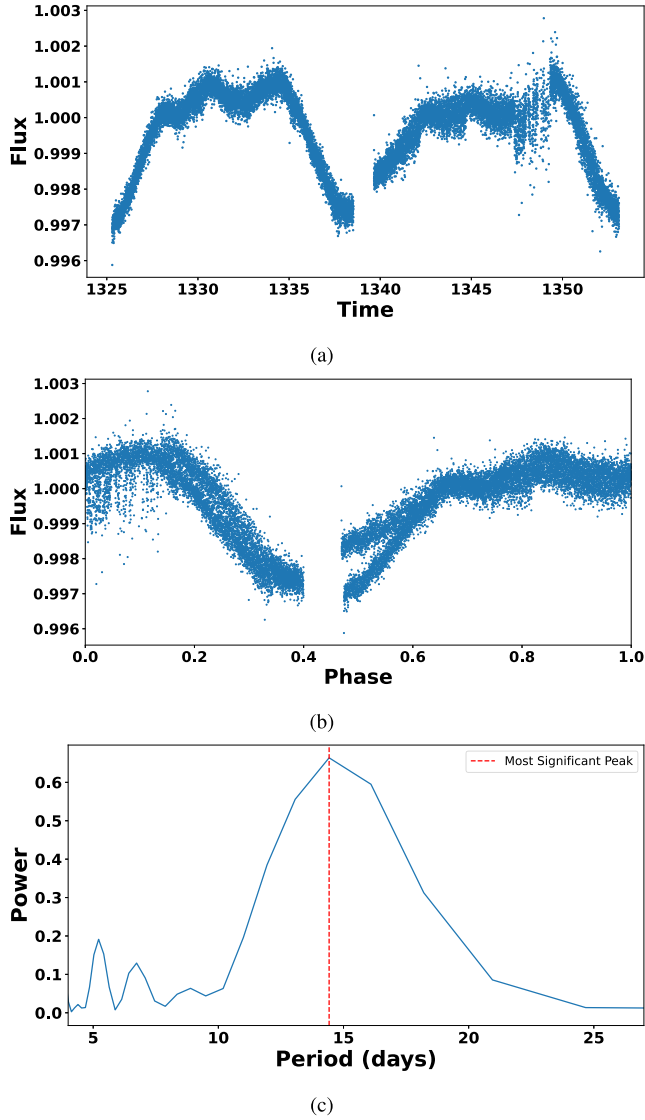
(a)

(b)

(c)

Figure 3. Panel (a) displays the *TESS* LC of HD 202628, illustrating the temporal variation in the star's flux as observed by *TESS*. Panel (b) exhibits the flux phase folding of HD 202628 over a period of 14.91 d. The Flux phase folding plot demonstrates a dip in brightness, indicating a significant variation occurring at this specific period. Panel (c) shows the LS periodogram derived from the *TESS* LC of HD 202628. The LS periodogram reveals the spectral power distribution of periodic signals present in the LC data. The most significant peak in this periodogram analysis is represented by the dotted line at a period of 14.91 ± 0.03 d.

index 4(c). Conservatively, we interpret this signal as indicative of possible activity rather than an exoplanet signal.

4 DISCUSSION

From our selection of 29 stars, we achieved successful validation of exoplanet signals for HD 10647, HD 115617, HD 69830, HD 142091, HD 22049, and GJ 581. Additionally, we refined the orbital parameters for exoplanets orbiting four specific stars − HD 10647, HD 115617, HD 22049, and HD 142091 − by employing a more extensive data set. Furthermore, through the utilization of the debris disc inclination angle for each star, we calculated M_{DA} of the exoplanets orbiting HD 10647, HD 115617, HD 69830, GJ 581, HD

(a)

(b)

(c)
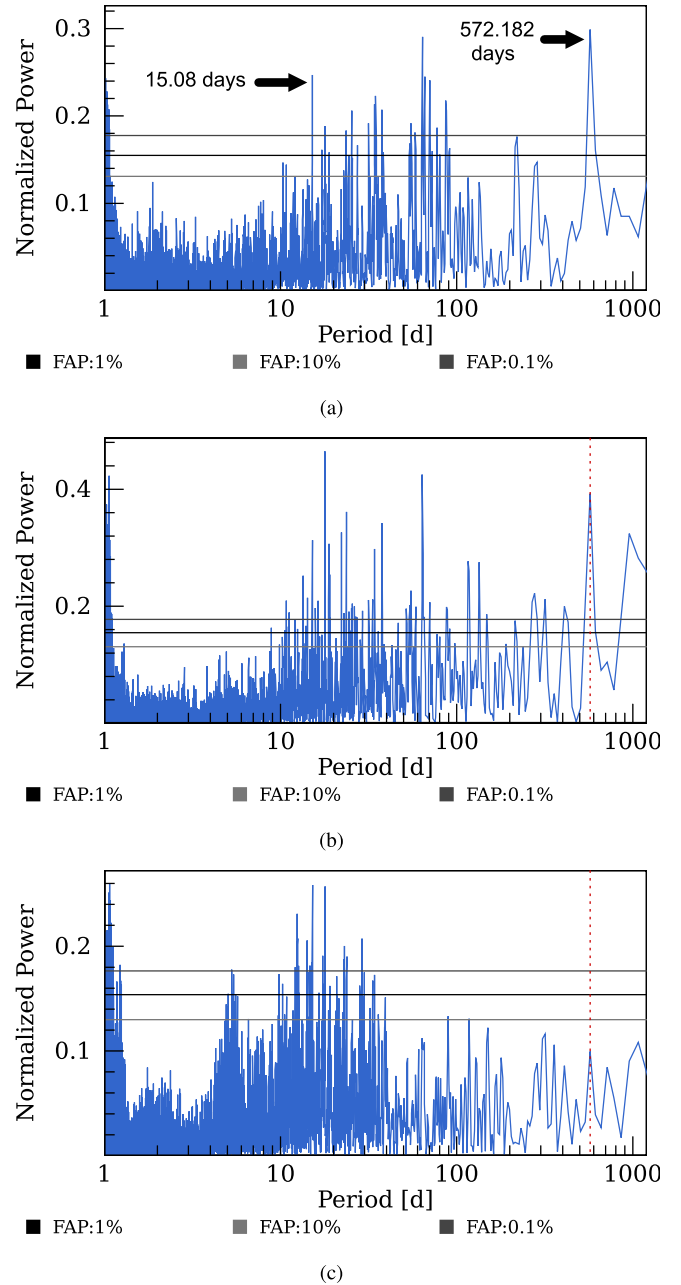
Figure 4. Panel (a): LS periodogram of the HARPS RV data set for HD 202628. The peak at 15.08 d corresponds to the rotational period, while the peak at 572.18 d indicates the presence of a potential exoplanet signal. Panel (b): LS Periodogram for S-Index indicator where dotted line denotes the 572.18 d signal. Panel (c): LS Periodogram for the BIS Indicator, with the 572.18-d period marked by the dotted line.

22049, and HD 142091. We have also detected long-term activity signals in HD 207129 and HD 202628. Finally, we compared our findings with prior studies. One of our assumptions was to consider disc–planet coplanarity and determine M_{DA}. Upon examining the results of HD 22049, we noticed that Feng et al. (2023) utilized astrometric data to compute the orbital inclination and calculate the mass of a planet. When comparing this mass value to the M_{DA} value of the planet detected around HD 22049, we find that the M_{DA} value of 0.70 ± 0.03 M_{Jup} closely aligns with the mass value of $0.76^{+0.14}_{-0.11}$ M_{Jup}, supporting our assumption of disc–planet coplanarity
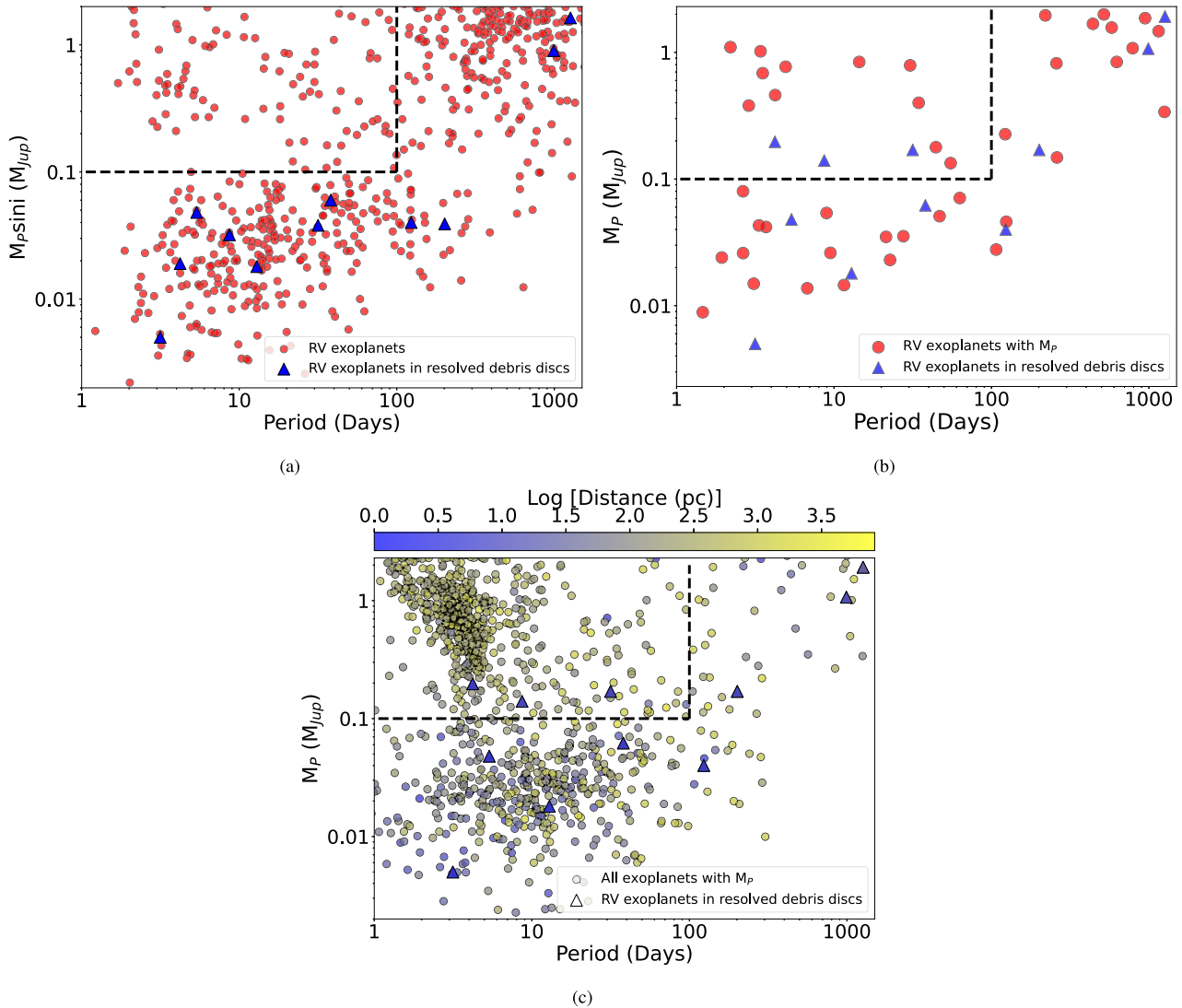
(a)

(b)

(c)

Figure 5. Panel (a): Scatter plot illustrating the correlation between $M_P \sin i$ and the orbital period. Circles represent RV-detected exoplanets sourced from the NASA Exoplanet Archive (Akeson et al. 2013), while triangles denote exoplanets detected within resolved debris discs as part of this study. The region marked by dotted lines indicates the area for warm and hot Jupiters. Panel (b): Scatter plot depicting the correlation between M_P and the orbital period, focusing exclusively on RV-detected exoplanets. Circles represent true masses sourced from the NASA Exoplanet Archive, while triangles signify M_{DA} of the RV-detected exoplanets discovered within the scope of this study. The region marked by dotted lines denotes the area for warm and hot Jupiters. Panel (c): Scatter plot to depict the correlation between M_P and the orbital period. Circles represent exoplanets for which true masses have been previously detected, sourced from the NASA Exoplanet Archive. Triangles depict M_{DA} of the RV-detected exoplanets within resolved debris discs as part of this study. The colour coding on this plot corresponds to the log of the stellar distance of the respective star around which the corresponding planet has been detected.

for estimating the closest mass approximation to the true mass of a planet. Furthermore, we observe that none of our young A−type stars exhibit any evidence of exoplanets when compared to solar-type stars. However, this absence may be attributed to detection bias; all of these stars have rapid rotation, which reduces radial velocity precision, as indicated by their high values of RV_{RMS} in Table 1.

Within our data set, five out of six stars with exoplanets harbour at least one low-mass planet with a minimum mass ($M_P \sin i$) of $\leq 30\, M_{Earth}$, and four out of these five stars have a metallicity ([Fe/H]) ≤ 0. This metallicity trend is consistent with the trends observed by Sousa et al. (2011) and Maldonado et al. (2012), which suggests that exoplanets hosting low-mass exoplanets tend to have a metallicity

less than solar. Referring to the predictions of Fernandes et al. (2019), the occurrence rate of exoplanets with masses ($M_P \sin i$) ranging from 0.1 to 20 M_{Jup} and orbital distances between 0.1 and 100 AU was 26.6 per cent$^{+7.5\ \text{per cent}}_{-5.4\ \text{per cent}}$. In our analysis, we have identified three exoplanets that fall within this range. Similarly, Mayor et al. (2009a) suggested that the occurrence rate of super-Earths and Neptunes (with $M_P \sin i = 3$–$30\, M_{Earth}$) having orbital periods of less than 50 d is estimated to be 30 per cent $\pm$ 10 per cent. Within our data set, five exoplanets fall within this specified range.

Maldonado et al. (2012) suggest that out of 29 planet-hosting stars with debris discs, 11 exhibit multiplanet systems, resulting in an incidence rate of 38 per cent. Similarly, Cao et al. (2023) report an incidence rate of 40 per cent, where out of 73 discs with

exoplanets, 29 host multiplanet systems. In our analysis, out of the seven planet-hosting stars we find with resolved debris discs, three of them host multiplanet systems. Additionally, Wolthoff et al. (2022) determined that the completeness-corrected global occurrence rate of giant planetary systems (systems with at least one planet with $M_P\sin i > 0.8\,M_{Jup}$) around evolved stars is 10.7 per cent$^{+2.2\text{ per cent}}_{-1.6\text{ per cent}}$. In comparison, within our data set of seven planetary systems, two exoplanets (HD 10647b, HD 142091 b) have $M_P\sin i$ greater than $0.8\,M_{Jup}$. The limited size of our data set constrains our ability to make strong conclusions about the exoplanet population surrounding debris discs. Overall, we do not find any significant indications of differences relative to earlier findings.

For visual analysis, we generated three scatter plots. The exoplanets selected for these plots share a common trait: they have a mass of less than $2\,M_{Jup}$ and an orbital period shorter than 1500 d. In Fig. 5(a), the filled red circles represent all RV-detected exoplanets, while the triangles represent RV-detected exoplanets in this study. This investigation is focused on RV-detected exoplanets accompanied by debris discs and demonstrates a distribution pattern akin to previously detected RV-detected exoplanets. In Fig. 5(a), the blue triangles align predominantly with regions that represent historically abundant areas of RV-detected exoplanets. In Figs 5(a), (b), and (c) we use black dashed lines for the area occupied by hot Jupiters and warm Jupiters. Hot Jupiters are planets with a short orbit, less than 10 d, and a planet mass greater than $0.1\,M_{Jup}$ (Wright et al. 2012; Yee et al. 2021) and have an occurrence rate ranging from 0.4 to 1.5 per cent (Cumming et al. 2008; Mayor et al. 2011; Howard et al. 2012; Fressin et al. 2013; Deleuil et al. 2018; Petigura et al. 2018; Kunimoto 2020; Beleznay & Kunimoto 2022). Warm Jupiters also have a planet mass greater than $0.1\,M_{Jup}$ but with orbits from 10 to 100 d (Huang et al. 2016; Wu et al. 2018). Dawson & Johnson (2018) suggests that warm Jupiters are less common than hot Jupiters. In our study, no exoplanets were detected within the demarcated region outlined by dashed lines in Fig. 5(a) until the correction for sin *i* is made in Figs 5(b) and (c).

In Fig. 5(c), the circles represent data extracted from the NASA Exoplanet Archive and include all exoplanets whose true masses have been determined either by a combination of the transit method and RV method, or by using the astrometric method and RV method. The triangles represent the M_{DA} of the RV-detected exoplanets in this study. The observations are colour-coded based on the stellar distances of the stars around which the exoplanets are detected. From the figure, it is apparent that the triangles represent exoplanets at much closer distances. So although the exoplanets detected around stars with debris discs are relatively few, they are among the closest examples of exoplanets with 'known' masses. It should be emphasized that the relatively high concentration of hot and warm Jupiter's in this plot arises due to the high sensitivity of transit surveys to detect such signals and not on their relative abundance.

We particularly note the three objects marked with blue triangles in Figs 5(b) and (c): HD 69830 b, HD 69830 c, and 61 Vir b. These objects have M_{DA} values that place them within the designated region for hot and warm Jupiters. This suggests that finding the orbital inclination angles of more RV-detected exoplanets could reveal additional planets in the hot and warm Jupiter zones. Additionally, Lin et al. (1996) proposed that hot Jupiters cannot form *in situ* but must migrate from the cold, icy regions of the protoplanetary disc, several astronomical units from the star. Since debris discs originate from protoplanetary discs, the detection of three planets in the hot and warm Jupiter zone may indicate nearby environments with relatively recent type-II disc migration. This highlights these planets as targets for studying planet migration in protoplanetary discs (Alibert et al. 2005).

DATA AVAILABILITY

All the data used for this research is based on publically available data. The information regarding debris discs is accessible through The Catalogue of Circumstellar Discs, which can be accessed at: https://www.circumstellardisks.org/. The *Transit Exoplanet Survey Satellite* (*TESS*) data employed in this study is available through the Mikulski Archive for Space Telescopes (MAST), accessible at: https://archive.stsci.edu/missions-and-data/tess. The RV data utilized in our study is derived from various repositories:

(i) The ESO archive, hosted by the European Southern Observatory, provides data at: https://www.eso.org/public/.

(ii) The Data Analysis Center for Exoplanets (DACE) project at the University of Geneva offers RV data through their Python API, accessible at: https://dace.unige.ch/pythonAPI/?tutorialId = 21.

(iii) The HARPS-RVBank archive, curated by the Max-Planck-Institut für Astronomie, can be accessed at: https://www2.mpia-hd.mpg.de/homes/trifonov/HARPS_RVBank.html.

(iv) Exostriker, a project hosted on GitHub by Trifon Trifonov, MPIA Heidelberg, provides RV data at: https://github.com/3fon3fonov/exostriker.

Lastly, historical exoplanet orbital parameter data are obtained from the NASA Exoplanet Archive, hosted by the California Institute of Technology. This archive can be accessed at: https://exoplanetarchive.ipac.caltech.edu/, and is operated under contract with the National Aeronautics and Space Administration (NASA).

REFERENCES

Akeson R. et al., 2013, PASP, 125, 989
Alibert Y., Mordasini C., Benz W., Winisdoerffer C., 2005, A&A, 434, 343
Allart R. et al., 2022, A&A, 666, A196
Anglada-Escudé G., Butler R. P., 2012, ApJS, 200, 15
Anna John A., Collier Cameron A., Wilson T. G., 2022, MNRAS, 515, 3975
Aumann H., 1985, PASP, 97, 885
Backman D. et al., 2008, ApJ, 690, 1522
Baines E. K., Armstrong J. T., Van Belle G. T., 2013, ApJ, 771, L17
Baliunas S. et al., 1995, ApJ, 438, 269
Ballard S. et al., 2013, ApJ, 773, 98
Barbato D. et al., 2023, A&A, 674, A114
Bean J. L., Benedict G. F., Endl M., 2006, ApJ, 653, L65
Beichman C. et al., 2005, ApJ, 626, 1061
Beichman C. et al., 2006, ApJ, 652, 1674
Beleznay M., Kunimoto M., 2022, MNRAS, 516, 75
Benedict G. F. et al., 2006, AJ, 132, 2206
Beuzit J.-L. et al., 2019, A&A, 631, A155
Bonfils X. et al., 2005, A&A, 443, L15
Bonsor A., Kennedy G. M., Crepp J. R., Johnson J. A., Wyatt M. C., Sibthorpe B., Su K. Y., 2013, MNRAS, 431, 3025
Booth M. et al., 2013, MNRAS, 428, 1263
Booth M. et al., 2016, MNRAS, 460, L10

Booth M. et al., 2017, MNRAS, 469, 3200
Booth M. et al., 2023, MNRAS, 521, 6180
Bouvier J. et al., 1999, A&A, 349, 619
Brogi M., Marzari F., Paolicchi P., 2009, A&A, 499, L13
Butler R. P. et al., 2006, ApJ, 646, 505
Butler R. P. et al., 2017, AJ, 153, 208
Cao P.-C., Liu Q., Liao N., Yang Q.-C., Huang D., 2023, A&A, 23, 085002
Castro-Ginard A. et al., 2024, A&A, 688, A1
Chambers J. E., 2004, Earth Planet. Sci. Lett., 223, 241
Coffinet A., Lovis C., Dumusque X., Pepe F., 2019, A&A, 629, A27
Cumming A., Butler R. P., Marcy G. W., Vogt S. S., Wright J. T., Fischer D. A., 2008, PASP, 120, 531
Dawson R. I., Johnson J. A., 2018, ARA&A, 56, 175
De Rosa R. J., Kalas P., 2019, AJ, 157, 125
Debes J. et al., 2023, ApJ, 948, 36
Deleuil M. et al., 2018, A&A, 619, A97
Demory B.-O. et al., 2009, A&A, 505, 205
Díaz R. et al., 2016, A&A, 591, A146
Díaz R. F., Almenara J. M., Santerne A., Moutou C., Lethuillier A., Deleuil M., 2014, MNRAS, 441, 983
Dupuy T. J., Kraus A. L., Kratter K. M., Rizzuto A. C., Mann A. W., Huber D., Ireland M. J., 2022, MNRAS, 512, 648
Eiroa C. et al., 2013, A&A, 555, A11
Engler N., Schmid H. M., Quanz S. P., Avenhaus H., Bazzon A., 2018, A&A, 618, A151
Faramaz V. et al., 2019, AJ, 158, 162
Favata F., Sciortino S., Micela G., 1997, A&A, 323, 809
Feng F., Butler R. P., Vogt S. S., Holden B., Rui Y., 2023, MNRAS, 525, 607
Feng F., Tuomi M., Jones H. R., Barnes J., Anglada-Escude G., Vogt S. S., Butler R. P., 2017, AJ, 154, 135
Fernandes R. B., Mulders G. D., Pascucci I., Mordasini C., Emsenhuber A., 2019, ApJ, 874, 81
Flores M., González J., Arancibia M. J., Saffe C., Buccino A., López F., Bustos R. I., Miquelarena P., 2018, A&A, 620, A34
Fressin F. et al., 2013, ApJ, 766, 81
Fulton B. J., Petigura E. A., Blunt S., Sinukoff E., 2018, PASP, 130, 044504
Gallenne A., Mérand A., Kervella P., Graczyk D., Pietrzyński G., Gieren W., Pilecki B., 2023, A&A, 672, A119
Gáspár A., Rieke G. H., Ballering N., 2016, ApJ, 826, 171
Goździewski K., Migaszewski C., 2018, ApJS, 238, 6
Grandjean A. et al., 2020, A&A, 633, A44
Gray R. O., Corbally C., Garrison R., McFadden M., Bubar E., McGahee C., O'Donoghue A., Knox E., 2006, AJ, 132, 161
Gray R. O., Corbally C., Garrison R., McFadden M., Robinson P., 2003, AJ, 126, 2048
Gray R. O., Kaye A. B., 1999, AJ, 118, 2993
Greaves J. S. et al., 2013, MNRAS, 438, L31
Green M. J., Maoz D., Mazeh T., Faigler S., Shahaf S., Gomel R., El-Badry K., Rix H.-W., 2023, MNRAS, 522, 29
Grunblatt S. K., Howard A. W., Haywood R. D., 2015, ApJ, 808, 127
Hatzes A. P. et al., 2000, ApJ, 544, L145
Heinze A., Hinz P. M., Kenworthy M., Miller D., Sivanandam S., 2008, ApJ, 688, 583
Hengst S., Marshall J. P., Horner J., Marsden S. C., 2020, MNRAS, 497, 1098
Hinkley S. et al., 2023, A&A, 671, L5
Hojjatpanah S. et al., 2020, A&A, 639, A35
Holmberg J., Nordström B., Andersen J., 2007, A&A, 475, 519
Howard A. W. et al., 2012, ApJS, 201, 15
Huang C., Wu Y., Triaud A. H., 2016, ApJ, 825, 98
Isaacson H., Fischer D., 2010, ApJ, 725, 875
Jenkins J. et al., 2006, MNRAS, 372, 163
Jenkins J. S. et al., 2015, MNRAS, 453, 1439
Johnson J. A., Marcy G. W., Fischer D. A., Wright J. T., Reffert S., Kregenow J. M., Williams P. K., Peek K. M., 2008, ApJ, 675, 784
Jones H. R., Butler R. P., Tinney C. G., Marcy G. W., Carter B. D., Penny A. J., McCarthy C., Bailey J., 2006, MNRAS, 369, 249
Kalas P. G. et al., 2015, ApJ, 814, 32
Keenan P. C., McNeil R. C., 1989, ApJS, 71, 245
Kennedy G. et al., 2012, MNRAS, 421, 2264
Kennedy G. M. et al., 2015, MNRAS, 449, 3121
Kennedy G., Wyatt M., Bryden G., Wittenmyer R., Sibthorpe B., 2013, MNRAS, 436, 898
Kiefer F., Hébrard G., Des Etangs A. L., Martioli E., Dalal S., Vidal-Madjar A., 2021, A&A, 645, A7
Kilic M., von Hippel T., Leggett S., Winget D., 2005, ApJ, 632, L115
Kluyver T. et al., 2016, Elpub, 2016, 87
Koerner D. et al., 2010, ApJ, 710, L26
Kraus S. et al., 2020, ApJ, 897, L8
Krist J. E. et al., 2010, AJ, 140, 1051
Krist J. E., Stapelfeldt K. R., Bryden G., Plavchan P., 2012, AJ, 144, 45
Krivov A. V., 2010, Res. Astron. Astrophys., 10, 383
Kunimoto M., 2020, PhD thesis, University of British Columbia
Lagrange A.-M. et al., 2016, A&A, 586, L8
Laliotis K. et al., 2023, AJ, 165, 176
Lawler S. et al., 2014, MNRAS, 444, 2665
Lestrade J.-F. et al., 2012, A&A, 548, A86
Li Y. et al., 2021, AJ, 162, 266
Lin D. N., Bodenheimer P., Richardson D. C., 1996, Nature, 380, 606
Liseau R. et al., 2008, A&A, 480, 799
Llop-Sayson J. et al., 2021, AJ, 162, 181
Lovell J. et al., 2021, MNRAS, 506, 1978
Luhn J. K., Wright J. T., Howard A. W., Isaacson H., 2020, AJ, 159, 235
MacGregor M. A. et al., 2017, ApJ, 842, 8
MacGregor M. A. et al., 2022, ApJ, 933, L1
Makarov V. V., Zacharias N., Finch C. T., 2021, Res. Notes Am. Astron. Soc., 5, 155
Maldonado J., Eiroa C., Villaver E., Montesinos B., Mora A., 2012, A&A, 541, A40
Maldonado J., Martínez-Arnáiz R., Eiroa C., Montes D., Montesinos B., 2010, A&A, 521, A12
Mamajek E. E., Hillenbrand L. A., 2008, ApJ, 687, 1264
Marmier M. et al., 2013, A&A, 551, A90
Marshall J. P. et al., 2011, A&A, 529, A117
Martínez-Arnáiz R., Maldonado J., Montes D., Eiroa C., Montesinos B., 2010, A&A, 520, A79
Martins B. C. et al., 2020, ApJS, 250, 20
Matrà L., Wyatt M. C., Wilner D. J., Dent W. R., Marino S., Kennedy G. M., Milli J., 2019, AJ, 157, 135
Mayor M. et al., 2009a, A&A, 493, 639
Mayor M. et al., 2009b, A&A, 507, 487
Mayor M. et al., 2011, preprint (arXiv:1109.2497)
Mayor M., Queloz D., 1995, Nature, 378, 355
Metchev S. A., Eisner J. A., Hillenbrand L. A., Wolf S., 2005, ApJ, 622, 451
Millar-Blanchaer M. A. et al., 2015, ApJ, 811, 18
Milli J. et al., 2017, A&A, 597, L2
Moór A. et al., 2015, MNRAS, 447, 577
Morales F., Bryden G., Werner M., Stapelfeldt K., 2016, ApJ, 831, 97
Mouillet D., Larwood J., Papaloizou J., Lagrange A., 1997, MNRAS, 292, 896
Mustill A. J., Wyatt M. C., 2009, MNRAS, 399, 1403
Nealon R., Pinte C., Alexander R., Mentiplay D., Dipierro G., 2019, MNRAS, 484, 4951
Nelson J. E., Mast T. S., Faber S. M., 1985, Keck observatory report, 90, 1
Nesvold E. R., Kuchner M. J., 2014, ApJ, 798, 83
Nowak M. et al., 2020, A&A, 642, L2
Oshagh M., Santos N. C., Boisse I., Boue G., Montalto M., Dumusque X., Haghighipour N., 2013, A&A, 556, A19
Pallé E. et al., 2020, A&A, 643, A25
Pasinetti-Fracassini L. E., Pastori L., Covino S., Pozzi A., 2001, A&A, 367, 521
Payne M. J., Ford E. B., Wyatt M. C., Booth M., 2008, in Proc. IAU Symp. 253, Dynamical Simulations of HD 69830 (vol. 4). Cambridge Univ. Press, Cambridge, p. 540
Pearce T. D. et al., 2022, A&A, 659, A135
Pearce T. D. et al., 2024, MNRAS, 527, 3876
Pearce T. D., Wyatt M. C., 2014, MNRAS, 443, 2541

Pepe F., Cameron A., Latham D., Molinari E., Udry S., 2013, Nature, 503, 377

Pérez S., Marino S., Casassus S., Baruteau C., Zurlo A., Flores C., Chauvin G., 2019, MNRAS, 488, 1005

Perrin M.-N., Cayrel de Strobel G., Dennefeld M., 1988, A&A, 191, 237

Petigura E. A. et al., 2018, AJ, 155, 89

Pilbratt G. et al., 2010, A&A, 518, L1

Pineda J. S., Youngblood A., France K., 2021, ApJ, 918, 40

Plavchan P. et al., 2020, Nature, 582, 497

Poblete P. P., Löhne T., Pearce T. D., Sefilian A. A., 2023, MNRAS, 526, 2017

Rajpaul V., Aigrain S., Osborne M. A., Reece S., Roberts S., 2015, MNRAS, 452, 2269

Refregier A., Douspis M., 2008, in Oschmann J. M., Jr., de Graauw M. W. M., MacEwen H. A., eds, Proc. SPIE Conf. Ser. Vol. 7010, Space Telescopes and Instrumentation 2008: Optical, Infrared, and Millimeter. SPIE, Bellingham, p. 383

Reidemeister M., Krivov A. V., Stark C. C., Augereau J.-C., Löhne T., Müller S., 2011, A&A, 527, A57

Reylé C., Jardine K., Fouqué P., Caballero J. A., Smart R. L., Sozzetti A., 2021, A&A, 650, A201

Ricker G. R. et al., 2010, American Astronomical Society Meeting Abstracts# 215, 450

Rivera E. J., Laughlin G., Butler R. P., Vogt S. S., Haghighipour N., Meschiari S., 2010, ApJ, 719, 890

Robertson P., Endl M., Cochran W. D., Dodson-Robinson S. E., 2013, ApJ, 764, 3

Rodet L., Beust H., Bonnefoy M., Lagrange A.-M., Galli P., Ducourant C., Teixeira R., 2017, A&A, 602, A12

Roettenbacher R. M. et al., 2021, AJ, 163, 19

Romaniello M., 2022, in The ESO science archive, Observatory Operations: Strategies, Processes, and Systems IX50. Vol. 12186, SPIE, the international society for optics and photonics, p. 101

Rosenthal L. J. et al., 2021, ApJS, 255, 8

Sakai N., Hanawa T., Zhang Y., Higuchi A. E., Ohashi S., Oya Y., Yamamoto S., 2019, Nature, 565, 206

Santos N. C., Israelian G., Mayor M., 2004, A&A, 415, 1153

Sato B. et al., 2012, PASJ, 64, 135

Schneider G. et al., 2006, ApJ, 650, 414

Schneider G. et al., 2014, AJ, 148, 59

Schneider G. et al., 2016, AJ, 152, 64

Ségransan D. et al., 2010, A&A, 511, A45

Sethi R., Martin D. V., 2024, MNRAS, 529, 4442

Simpson E. K., Baliunas S. L., Henry G. W., Watson C. A., 2010, MNRAS, 408, 1666

Soummer R. et al., 2014, ApJ, 786, L23

Sousa S. G., Santos N. C., Israelian G., Mayor M., Udry S., 2011, A&A, 533, A141

Spronck J. F., Fischer D. A., Kaplan Z. A., Schwab C., Szymkowiak A., 2013, PASP, 125, 511

Stempels H., Gahm G., Petrov P., 2007, A&A, 461, 253

Stencel R. E., Backman D. E., 1991, ApJS, 75, 905

Suárez Mascareño A., Rebolo R., González Hernández J. I., Esposito M., 2017, MNRAS, 469, 4268

Tal-Or L., Trifonov T., Zucker S., Mazeh T., Zechmeister M., 2019, MNRAS, 484, L8

Tanner A. et al., 2015, ApJ, 800, 115

The Extrasolar Planet Encyclopaedia, 2023, The Extrasolar Planet Encyclopaedia. Available at: http://exoplanet.eu/

Toledo-Padrón B. et al., 2019, MNRAS, 488, 5145

Torres C., Quast G., Da Silva L., de La Reza R., Melo C., Sterzik M., 2006, A&A, 460, 695

Traub W., Shaklan, S., Lawson P., 2007, in Kalas P., ed., In the Spirit of BernardLyot: The Direct Detection of Planets and Circumstellar Disks in the 21stCentury. p. 24

Trifonov T. et al., 2018, A&A, 609, A117

Trifonov T., 2019, Astrophysics Source Code Library, record ascl–1906

Trifonov T., Tal-Or L., Zechmeister M., Kaminski A., Zucker S., Mazeh T., 2020, A&A, 636, A74

Tuomi M. et al., 2013, A&A, 551, A79

Udry S. et al., 2007, A&A, 469, L43

Vallenari A. et al., 2023, A&A, 674, A1

Van Leeuwen F., 2007, A&A, 474, 653

Vanderburg A., Plavchan P., Johnson J. A., Ciardi D. R., Swift J., Kane S. R., 2016, MNRAS, 459, 3565

VanderPlas J. T., 2018a, PASP, 130, 064502

VanderPlas J. T., 2018b, ApJS, 236, 16

Vogt S. S. et al., 2009, ApJ, 708, 1366

Vogt S. S. et al., 2014, PASP, 126, 359

Vogt S. S., Butler R. P., Rivera E. J., Haghighipour N., Henry G. W., Williamson M. H., 2010, ApJ, 723, 954

Von Braun K. et al., 2014, MNRAS, 438, 2413

Watson C., Littlefair S., Diamond C., Cameron A. C., Fitzsimmons A., Simpson E., Moulds V., Pollacco D., 2011, MNRAS, 413, L71

Wenger M. et al., 2000, A&AS, 143, 9

Werner M. W. et al., 2004, ApJS, 154, 1

White T. R. et al., 2018, MNRAS, 477, 4403

Wolthoff V., Reffert S., Quirrenbach A., Jones M. I., Wittenmyer R. A., Jenkins J. S., 2022, A&A, 661, A63

Wright J., Marcy G., Howard A., Johnson J. A., Morton T., Fischer D., 2012, ApJ, 753, 160

Wu D.-H., Wang S., Zhou J.-L., Steffen J. H., Laughlin G., 2018, AJ, 156, 96

Wyatt M. C., Jackson A. P., 2016, Space Sci. Rev., 205, 231

Wyatt M. et al., 2012, MNRAS, 424, 1206

Xiang-Gruess M., Papaloizou J. C., 2013, MNRAS, 431, 1320

Xiao G.-Y. et al., 2023, Res. Astron. Astrophys., 23, 055022

Xuan J. W., Kennedy G. M., Wyatt M. C., Yelverton B., 2020, MNRAS, 499, 5059

Yahalomi D. A., Angus R., Spergel D. N., Foreman-Mackey D., 2023, AJ, 166, 258

Yee S. W., Winn J. N., Hartman J. D., 2021, AJ, 162, 240

Zechmeister M. et al., 2013, A&A, 552, A78

Zechmeister M. et al., 2018, A&A, 609, A12

Zhu Z., 2019, MNRAS, 483, 4221

Zurlo A. et al., 2018, MNRAS, 480, 35

This paper has been typeset from a TeX/LaTeX file prepared by the author.